AIMS Biophysics

AIMS Biophysics, 12(1): 101−120.
DOI: 10.3934/biophy.2025007
Received: 01 December 2024
Revised: 27 January 2025
Accepted: 17 February 2025
Published: 17 March 2025

http://www.aimspress.com/journal/biophysics

Research article

Determination of the concentrations of possible endogenous photosensitizers in *Candida auris* via two-dimensional fluorescence spectroscopy

Anna-Maria Gierke*, Robin Haag and Martin Hessling

Institute of Medical Engineering and Mechatronics, Ulm University of Applied Sciences, Albert-Einstein-Allee 55, D-89081 Ulm, Germany

* **Correspondence:** Email: anna-maria.gierke@uni-ulm.de; Tel: +9647504683697.

Abstract: *Candida auris* is an emerging pathogenic yeast. In order to investigate possible light-based disinfection systems or therapeutic approaches, this study examined the formation of possible photosensitizers under different growth conditions. The yeast was cultivated under aerobic conditions in YEPG medium and minimal medium with 10% NaCl. 2D fluorescence spectroscopy (15 excitation wavelengths from 320 to 450 nm) at different time points was performed to calculate the concentrations and proportions of dry mass of various fluorophores. Comparing the different growth conditions, higher concentrations of porphyrins were observed with minimal medium + 10% NaCl than with the YEPG medium. When determining the concentrations of different fluorophores over time, different dynamics could be observed for both aerobic growth conditions. For both growth conditions, NADH, followed by thiamine and lumichrome, exhibited the highest concentrations; coproporphyrin III showed the lowest.

Keywords: photosensitizer; fluorophores; fluorescence measurements; concentration; ROS; flavin; porphyrin

1. Introduction

Candida auris is an emerging pathogenic yeast that has already been categorized as having high priority by the Centers for Disease Control and Prevention and the WHO due to invasive infections [1,2].

Cases of nosocomial infections in hospitals and healthcare facilities are rising. Ear, wound, bloodstream, urinary tract, and respiratory tract infections can be caused by *C. auris*. Furthermore, multi-resistance to antimycotics is increasingly being reported [3,4].

A certain morphology variance of *C. auris* has been described, with the yeast commonly characterized as being round shaped [5–7]. However, aggregates and an elongated shape can be observed as a result of stress factors, as investigated by Wang et al. by adding NaCl to the growth medium [6]. *C. auris* can be found on the skin in coexistence with other bacteria and fungi [8]. Different areas of skin on the body can be distinguished by their moisture degree, increased sweat, and sebaceous glands [9]. Skin areas with increased sweat glands, for example, have an increased salt content [10,11]. *C. auris* has been detected on various areas of the skin, such as the armpit, groin, nose, ear canal, fingertip, palm, nail, and perianal skin [12,13].

As *C. auris* and many other microorganisms are pathogenic, it is important to investigate new inactivation techniques. In addition to drug treatment approaches or chemical methods, visible light photoinactivation is another possibility. This is based on the excitation of so-called photosensitizers (PSs), which are usually also fluorophores. While exogenous PSs are applied in photodynamic therapy (PDT), endogenous PSs include, for example, porphyrins, which are found in heme biosynthesis (cytosol and mitochondria) [14]. Several studies have described the application of endogenous porphyrins in fluorescence diagnostics (FD) and PDT [15–17]. Furthermore, endogenous PSs also include flavins [18–20], among which FMN and FAD can be detected in yeast cells in addition to riboflavin, as described in the study by Pallota 2011 using *S. cerevisiae* [21]. These substances can hardly be distinguished spectrally using fluorescence measurements [22,23].

PSs are excited by the absorption of a photon and thus change from the ground singlet state to the excited singlet state and can then transfer to the long-lived triplet state [24]. Two types of reaction can then take place, resulting in the formation of reactive oxygen species (ROS). In type I reactions, electrons are transferred to oxygen, resulting in the formation of ROS such as superoxide radicals, hydroxyl radicals, and others. Further ROS can then be formed via the Haber–Weiss reaction using these superoxide radicals [25]. Singlet oxygens can be formed in type II reactions via the transfer of energy. ROS can be formed in various cell components such as the cell membrane, cytosol, peroxisomes, endoplasmic reticulum, or membranes of mitochondria [26].

After fluorophores have been excited by photons and thus raised to the excited singlet state, they can return to the ground singlet state by fluorescence [27]. A further possibility of emission is via phosphorescence after the excited fluorophore has entered the long-lived triplet state and then changed to the ground singlet state.

As there is a tendency for drug resistance to increase in *C. auris*, this yeast should be further investigated regarding visible light photoinactivation. For this, various possible PSs were investigated using fluorescence measurements to determine which fluorophores can be formed and thus measured under which growth conditions. The experiments were carried out aerobically with either YEPG or a minimal medium and an additional 10% NaCl for increased salt stress. Furthermore, to determine how the formation of different fluorophores changes over time of cultivation, fluorophore proportions were calculated for each measuring point using the time course of the measured fluorescence spectra.

The aim of this study is to investigate which fluorophores or possible PSs can be found in *C. auris*. Differences due to different growth conditions will be observed, as will the determination of the respective concentrations and changes over time.

2. Materials and methods

C. auris (DSM 21092) was chosen to investigate possible endogenous PSs and development over time during growth phases.

The yeast was cultivated in liquid culture for both growth investigations and fluorescence measurements. A modified form of yeast extract peptone glucose (YEPG) medium was chosen [200 mL glucose (250 g/L), 20 g peptone from casein, and 10 g yeast extract per 1,000 mL; pH 6.5]. Samples were spread out on potato dextrose agar plates. The minimal medium (reduced nutrient content compared to the modified YEPG medium) consisted of 0.5% peptone from casein and 0.1% Tween 80. As a further stress factor, 10% NaCl was added [6,28].

For growth curves, a sample was taken from a preculture prepared 24 h earlier with YEPG medium at 30 °C and transferred to the desired amount of the respective medium (1: 150). After different time points, samples were taken from these cultures in different media to measure the optical density at 600 nm (OD_{600nm}) with a spectrophotometer (SPECORD 250 PLUS double beam spectrophotometer, Analytik Jena, Germany). Colony-forming units per milliliter (CFU/mL) were also determined. For this purpose, samples were centrifuged at 7,000 × g for 5 min and the resuspension was washed twice with phosphate-buffered saline (PBS). The resulting suspension was plated on agar plates and analyzed by counting visible colonies after 48 h of incubation. In addition, images were taken with a microscope (Nikon Eclipse TE2000-U and Nikon D5600, Nikon, Japan) at 60 × and 100 × magnification.

For fluorescence measurements, liquid cultures were prepared at a ratio of 1: 150 to the YEPG medium preculture. From this, the respective amount of preculture was added to the respective medium. Various samples were taken at different times. The optical density at 600 nm (OD_{600nm}) was measured and yeast concentration was determined. Samples were washed under resuspension with PBS and centrifuged at 7,000 × g for 5 min, and the supernatant was discarded. To determine dry mass, autoclaved distilled water was added to the sample to obtain a defined concentration, and three samples (1 mL each of the suspension) were taken. These samples were dried; after weighing, the resulting masses were averaged. The suspension sample was centrifuged again at 7,000 × g for 5 min, and the remaining supernatant was measured. The amount of supernatant was again added as Laemmli buffer with a pH of 6.8 [29]. The resulting suspension was heated to 90 °C for 5 min and centrifuged again. The supernatant was used for fluorescence measurements using a microtiter plate (MTP) reader (CLARIOstar® plus, BMG LABTECH GmbH, Germany). The following settings were chosen for the MTP reader: photomultiplier gain 2.000, focal height 6.5 mm, settling time 0.5 s, temperature 30 °C. A sample volume of 100 µL was added to the wells of the 96-well MTP.

In order to investigate the concentrations of possible PSs, these were examined for fluorescence at different excitation wavelengths (320, 330, 340, 350, 355, 360, 365, 370, 380, 390, 400, 410, 420, 430, and 450 ± 8 nm). All PSs were dissolved in DMSO [dimethyl sulfoxide; C_2H_6OS, purity (GC) > 99%, CAS: 67–68–5, SERVA Electrophoresis GmbH, Germany] with the exception of NADH (β-nicotinamide adenine dinucleotide reduced disodium salt, $C_{21}H_{27}N_7Na_2O_{14}P_2$, purity 97%, CAS: 606–68–8, Alfa Aesar, USA, dissolved in distilled water) and thiamine (dissolved in Ringer's solution). PSs were further diluted with Laemmli buffer (**Table 1**). The following fluorophores were selected [30–32]: Rbf-eq. (flavins/riboflavin-equivalent; riboflavin, $C_{17}H_{20}N_4O_6$, purity 98%, CAS: 83–88–5, Alfa Aesar, USA), Lmc (lumichrome; $C_{12}H_{10}N_4O_2$, CAS: 1086–80–2, Merck KGaA, Germany), NADH, PPIX [protoporphyrin IX; $C_{34}H_{34}N_4O_4$, purity (HPLC) > 98%, CAS: 553–12–8, Santa Cruz

Biotechnology Inc., USA], ZnPP [zinc-protoporphyrin; $C_{34}H_{32}N_4O_4Zn$, purity (TLC) 96%, CAS: 15442–64–5, Alfa Aesar, USA], Copro III [coproporphyrin III dihydrochloride; $C_{36}H_{38}N_4O_8 \cdot 2HCL$, purity (HPLC) 98.5%, CAS: 14643–66–4, Santa Cruz Biotechnology Inc., USA], and Thm (thiamine chloride hydrochloride; $C_{12}H_{17}CIN_4OS \cdot HCL$, purity > 98%, CAS: 67–03–8, Merck KGaA, Germany). Both the *C. auris* and fluorophores samples were maintained in the dark until the start of the measurements to prevent possible bleaching. Fluorescence spectroscopy was carried out for yeast samples or the fluorophores in triplicates and six-fold for the reference samples (distilled water, DMSO, Laemmli buffer, and an empty well plate). Growth experiments were repeated three times. The contour plots of fluorophores and yeast samples were created with Origin 2021b (OriginLab Corporation, Northampton, MA, USA).

Table 1. Overview of final concentrations of the chosen fluorophores, presenting the concentration of each excitation wavelength for the fluorophores.

	Concentration (µg/mL)						
Excitation wavelength (nm)	Rbf-eq.	Lmc	NADH	PPIX	ZnPP	Copro III	Thm
320	15	240	28	80	16	12	52
330	15	240	28	80	16	12	52
340	15	24	28	80	16	12	52
350	15	24	28	80	16	12	52
355	1.5	24	28	80	16	12	52
360	1.5	24	28	16	16	12	52
365	1.5	24	28	16	16	12	52
370	1.5	24	28	16	16	12	52
380	1.5	24	28	16	8	12	52
390	1.5	24	28	8	8	12	52
400	1.5	24	140	8	8	12	52
410	1.5	24	140	8	8	12	52
420	1.5	24	140	8	8	12	52
430	1.5	240	140	8	8	12	52
450	1.5	240	140	8	8	12	52

Fluorescence measurements aimed at investigating the extent to which tested fluorophores occur in the yeast samples examined; thus, the concentrations of the fluorophores were determined. For this purpose, the samples of both *C. auris* and fluorophores were excited at different wavelengths as mentioned above.

Initially, the respective proportions of the fluorescence spectra from Laemmli buffer and DMSO or distilled water were subtracted from the averaged fluorescence spectra according to **Table 1**. This procedure reduced the overall number of fit parameters required and helped in the optimization of unknown contributors to the fluorescence spectrum. For thiamine, data from water and the empty well plate were subtracted. Fluorophore and sample data were linearly interpolated for a single excitation wavelength and fitted to the data of the same excitation wavelength of the yeast sample using the least

squares method with the following fit function (**Formula 1**). For this purpose, the yeast sample data were not interpolated beforehand.

$$F(\lambda) = \sum_{n=0}^{N} A_n f_n(\lambda) \; ; \; A_n \in \mathbb{R}, N \in \mathbb{N} \tag{1}$$

A_n: constants; $f_n(\lambda)$: interpolation of the data from fluorophores; photon counts; λ: emission wavelength; N: number of fluorophores.

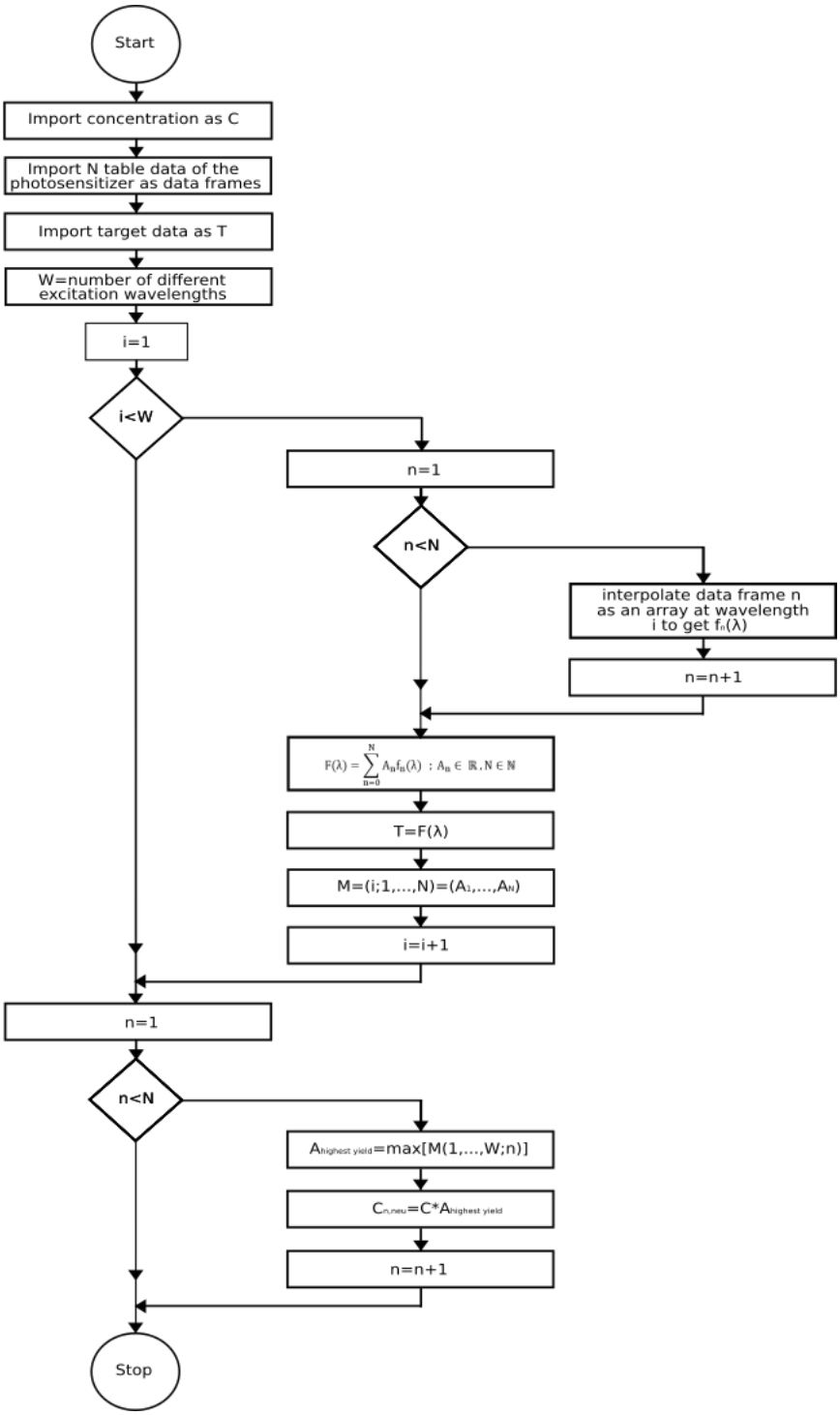

Figure 1. Flowchart for calculating the concentrations of fluorophores in samples of *C. auris*.

All constants were saved to a parameter matrix. The concentrations from Table 1 were then multiplied with the constants from the fit at their respective excitation wavelengths. The calculation was performed with Python 3.8.

3. Results

In order to examine the fungal samples, fluorophores were excited with different wavelengths (320, 330, 340, 350, 355, 360, 365, 370, 380, 390, 400, 410, 420, 430, and 450 ± 8 nm) and the emission curves were presented graphically (**Figure 2**). Riboflavin-equivalent had a peak at an emission wavelength of 520–530 nm. A peak was observed at approximately 450–465 nm for lumichrome, at 440–470 nm for thiamine, and at 440–480 nm for NADH. For protoporphyrin IX, peaks were detected at approximately 630–640 nm and 690–710 nm. For zinc-protoporphyrin, peaks were measured at 585–595 nm and 635–650 nm; for coproporphyrin III, peaks were detected at 610–620 and 660–680 nm.

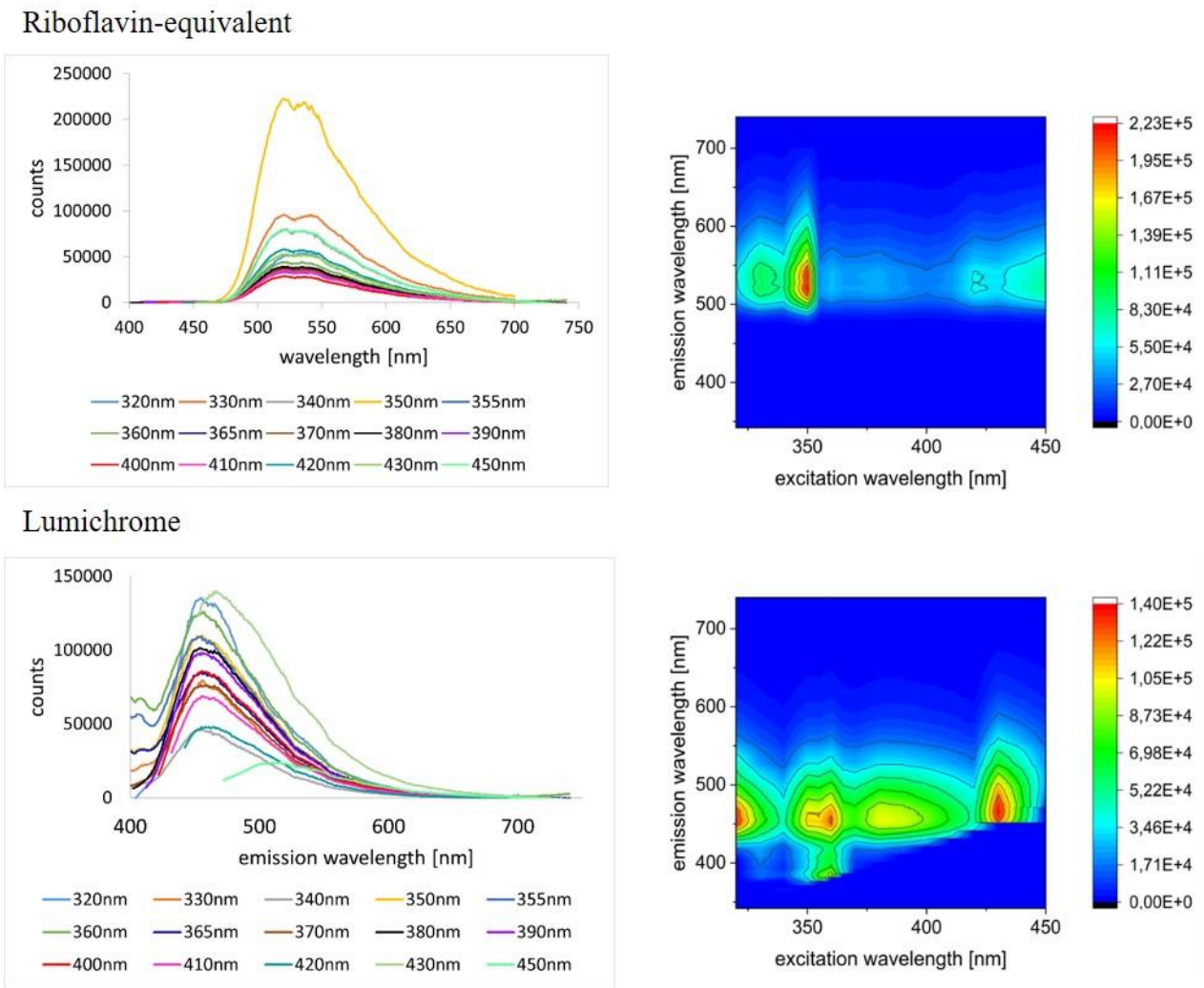

NADH

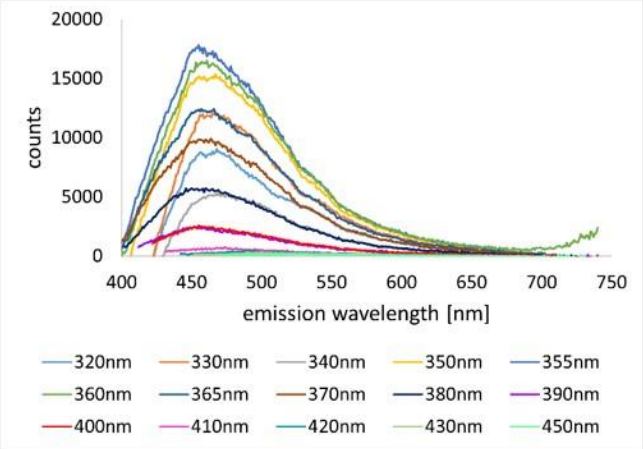

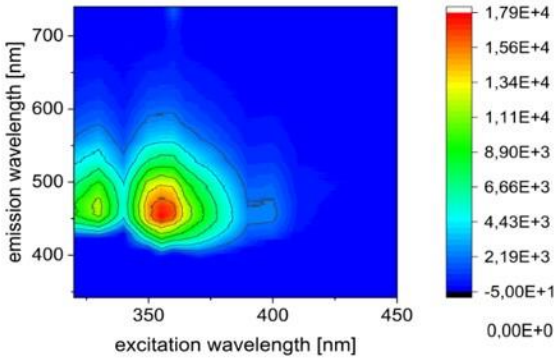

Protoporphyrin IX

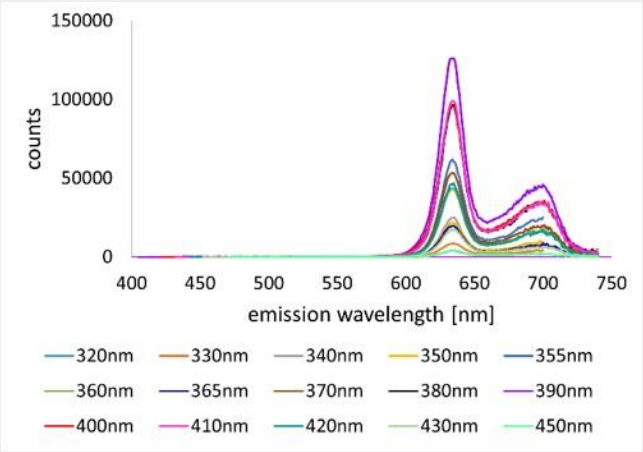

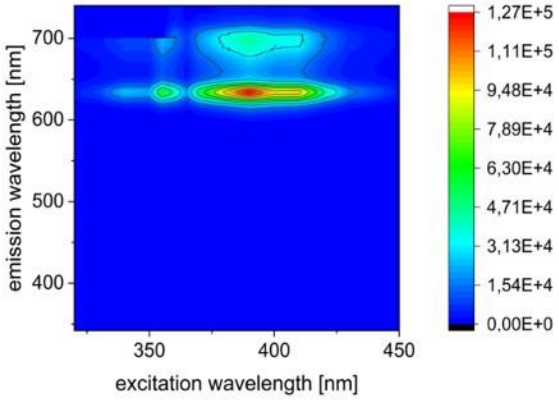

Zinc-protoporphyrin

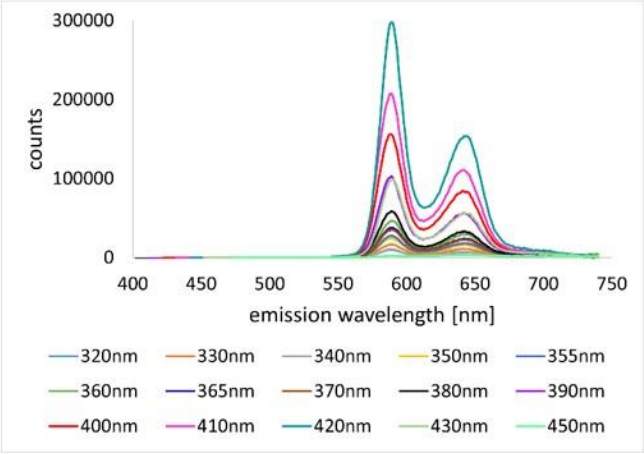

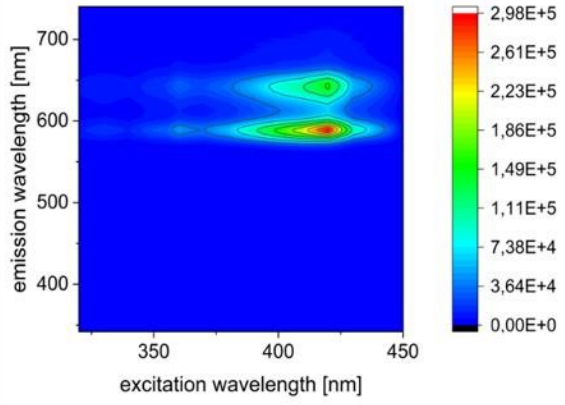

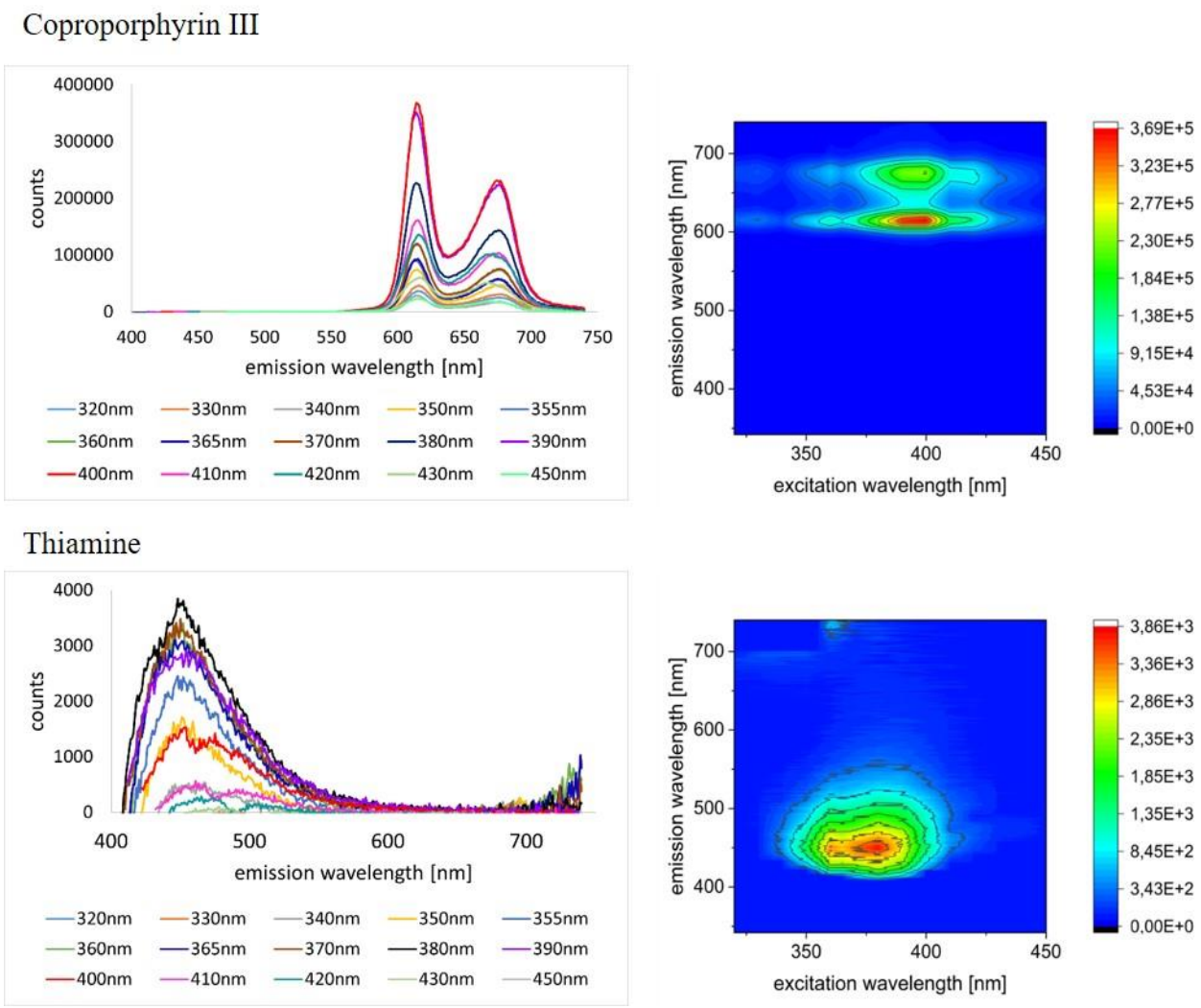

Figure 2. Fluorescence spectra of all investigated fluorophores (pure chemicals) in suspension with different excitation wavelengths (320–450 nm). The concentrations selected for measurement are presented in Table 1.

3.1. Studies on different growth conditions

For the following investigations, two growth conditions were applied: cultivation with YEPG medium after 48 h and cultivation with minimal medium + 10% NaCl after 44 h. **Figure 3** presents the microscopic images of both cultures. During growth in YEPG medium, single yeast cells or still-connected mother–daughter cells were observed. After growth with minimal medium + 10% NaCl, yeast aggregates were predominantly found.

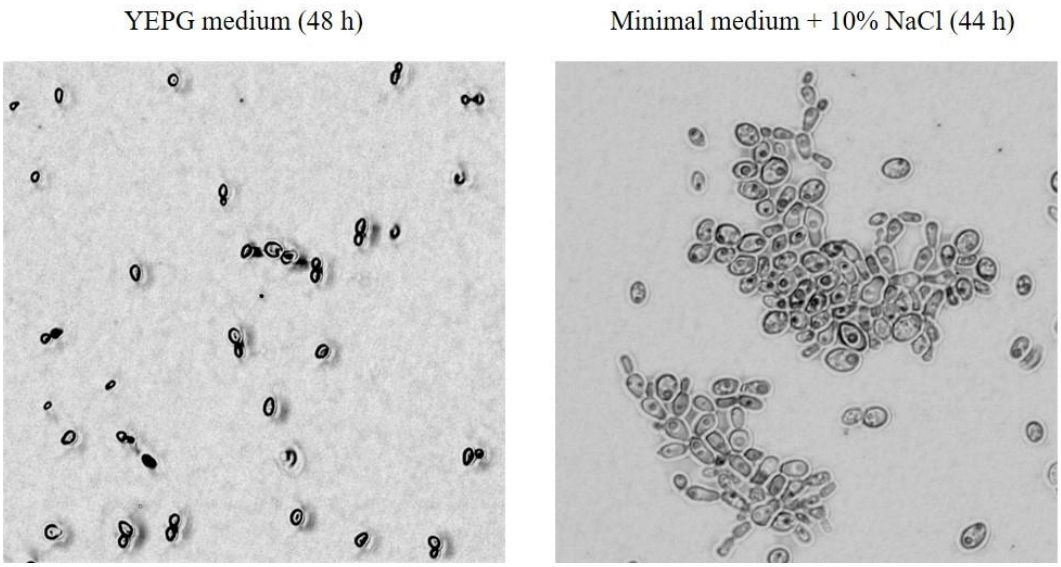

Figure 3. Microscopic images of *C. auris*. Cultures were cultivated aerobically in YEPG medium (48 h) or in minimal medium + 10% NaCl (44 h). Magnification: 60 × (left) and 100 × (right).

Figure 4 presents fluorescence spectra of *C. auris* samples at different excitation wavelengths. During growth with YEPG medium, emission peaks at 430–450 nm and 500–550 nm were observed after 48 h, where the second peak had higher counts at excitation wavelengths of 420, 430, and 450 nm than the first peak. In fluorescence measurements of the yeast samples grown in minimal medium + 10% NaCl, peaks were also detected at 430–450 nm and 500–550 nm, but also at 575–585 nm and 630–640 nm.

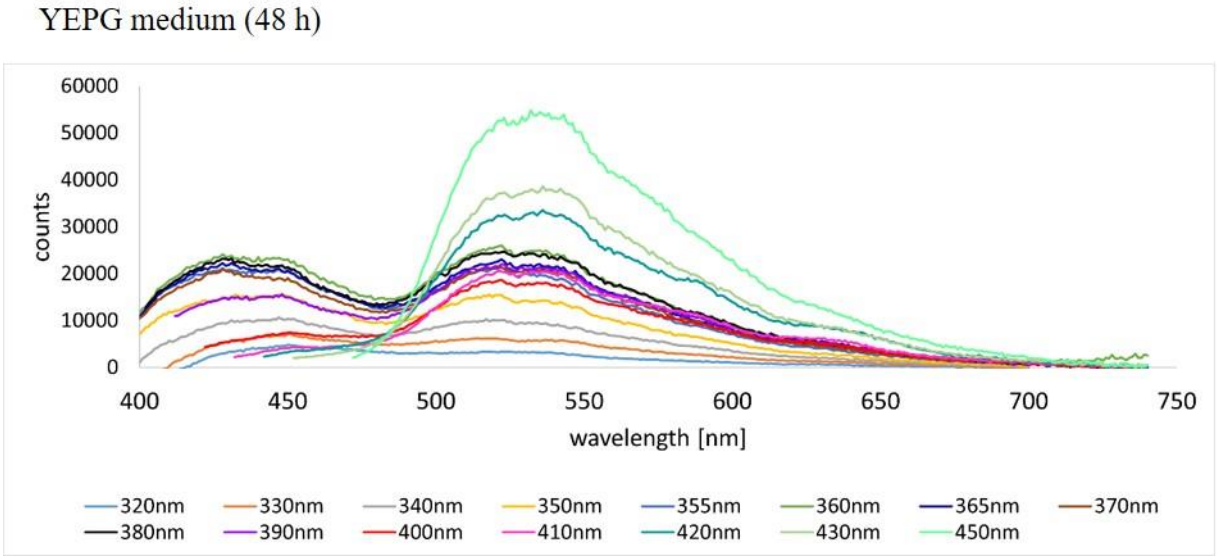

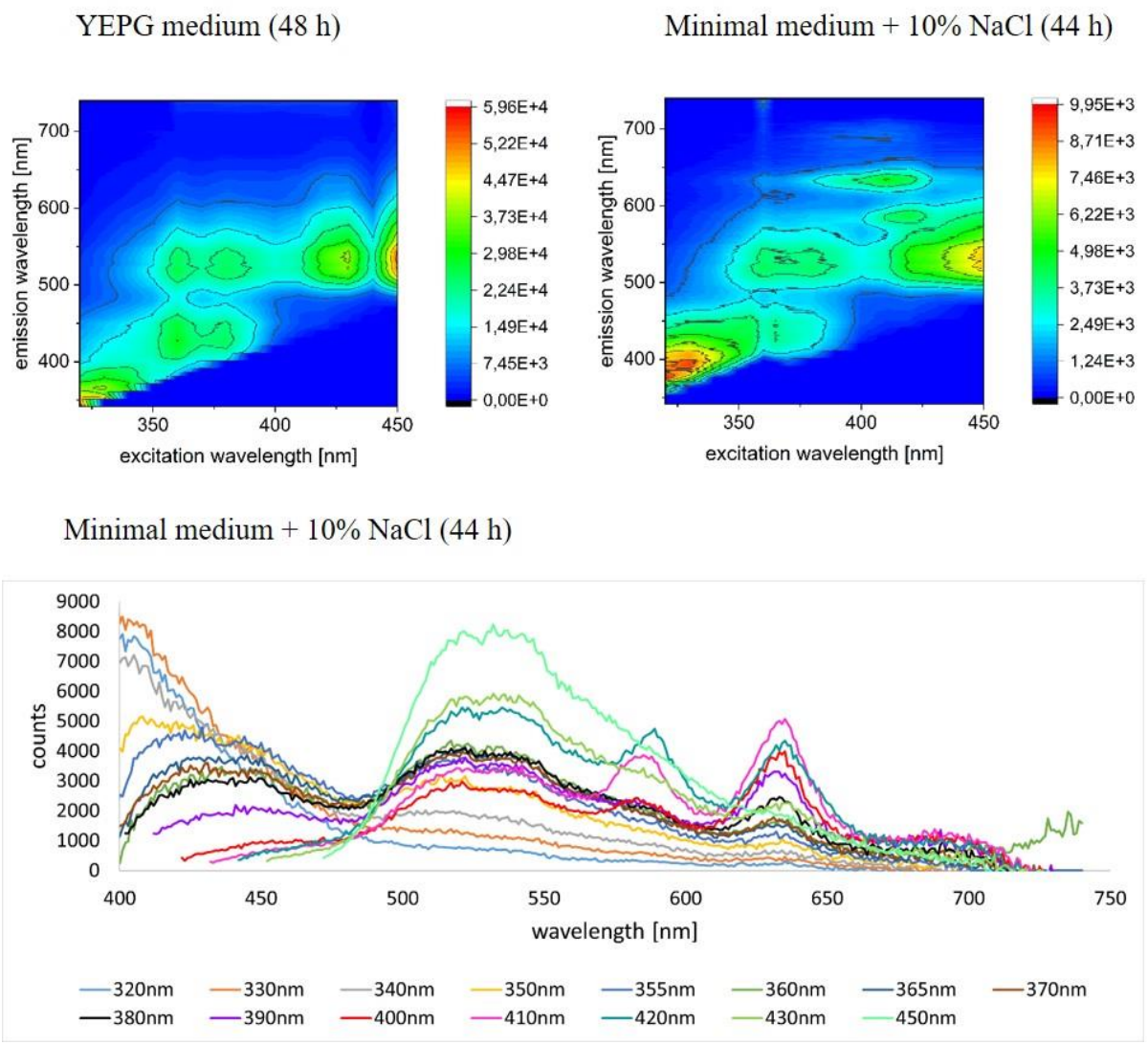

Figure 4. Fluorescence spectra of *C. auris* under different growth conditions with different excitation wavelengths (320, 330, 340, 350, 355, 360, 365, 370, 380, 390, 400, 410, 420, 430, and 450 ± 8 nm).

3.2. Growth experiments

To investigate the development of fluorophores over time, growth curves were initially carried out by OD_{600nm} measurements (**Figure 5**). The experiments were carried out in YEPG medium and in minimal medium + 10% NaCl. An OD_{600nm} value of 6.7 was achieved after growth in YEPG medium after 48 h; an OD_{600nm} value of 0.17 was found after growth in minimal medium + 10% NaCl after 44 h.

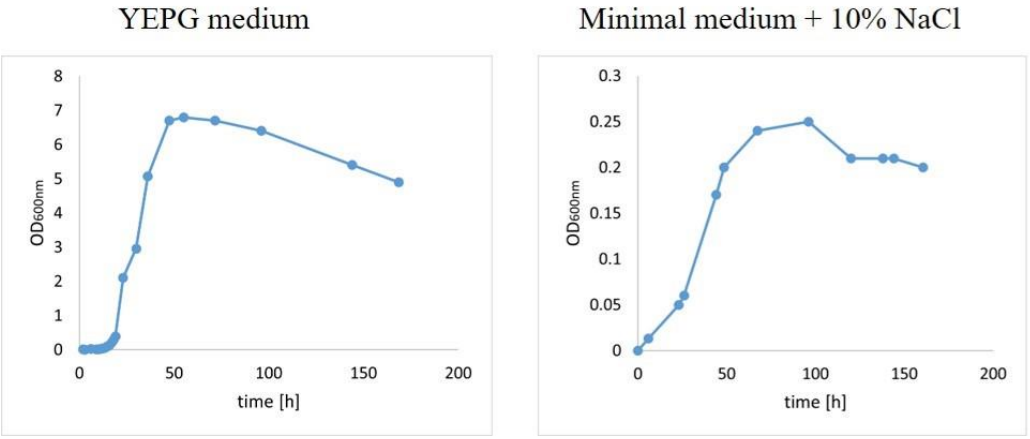

Figure 5. Growth curves of *C. auris* under different growth conditions: YEPG medium and minimal medium + 10% NaCl.

Figure 6 presents the concentrations of various fluorophores over time and under different aerobe growth conditions. During growth in YEPG medium, the concentration of NADH and Lmc continued to increase until the end of the growth experiment. With PPIX, a sharp increase was observed after a few hours, followed by a decrease before 50 h. The concentrations of other fluorophores increased until 100 h, with fewer concentration changes afterward.

In the fluorescence measurements with yeast samples grown in minimal medium + 10% NaCl, concentration increased for all fluorophores up to 44 h. Thereafter, a smaller increase or a decrease was observed over time. After 72 h, an increase in the concentration of Lmc, Thm, and NADH was detected. The concentration of ZnPP increased up to 72 h and then decreased.

Under both growth conditions, NADH presented the highest concentration, followed by Thm and Lmc; Copro III had the lowest concentration. NADH had a concentration of 461 ± 55 μg/mL for growth with YEPG medium after 150.5 h and 139 ± 15 μg/mL for growth with minimal medium + 10% NaCl after 160.5 h (**Table 2**).

The growth experiments were repeated with both cultivation media, and the dry mass of each yeast sample was determined at different time points. From the determined concentrations of fluorophores and dry mass, the proportion to dry mass could be calculated (**Table 2**). An increase in dry mass was observed over time for all samples with both media (excluding 160.5 h cultivation with minimal medium + 10% NaCl). The dry mass of the yeast sample was 117 ± 4 mg/mL after 72 h with YEPG medium and 29 ± 5 mg/mL after 72 h with minimal medium + 10% NaCl. Under both growth conditions, NADH and thiamine were calculated with the highest proportion to dry mass. A proportion to dry mass of (50 ± 15) × 10^{-4} was determined for NADH after 20 h with YEPG medium and 13 ± 4 × 10^{-2} after 22 h with the other medium. For thiamine, the highest proportion after 48 h with YEPG medium was (261 ± 16) × 10^{-5}; with minimal medium + 10% NaCl, the maximum proportion after 22 h was (47 ± 16) × 10^{-3}.

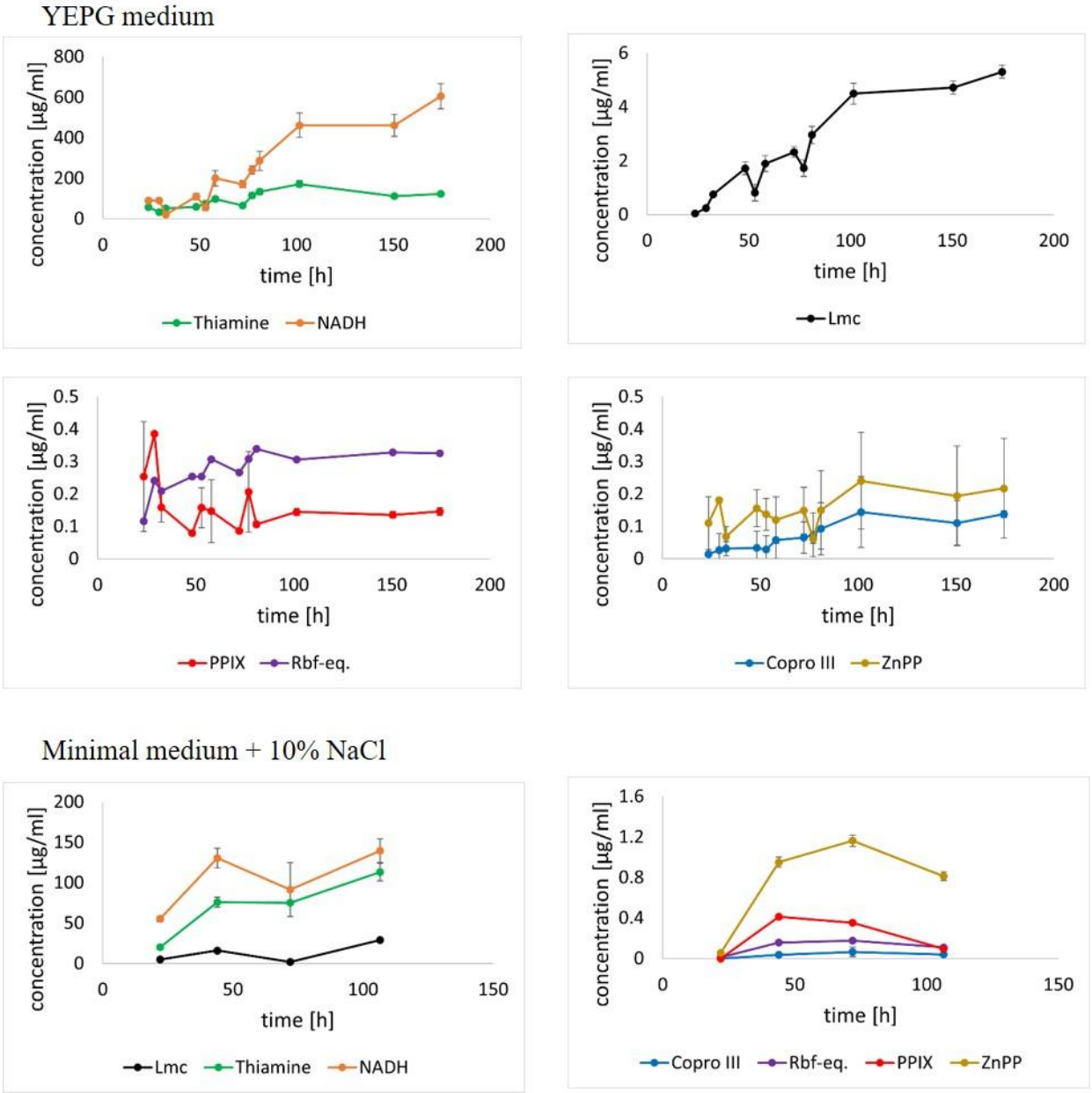

Figure 6. Concentration of different fluorophores over time under different growth conditions: YEPG medium and minimal medium + 10% NaCl. A major contributor to the presented error bars is the computational error arising in the numerical application of the fit with Formula 1.

Table 2. Concentrations of investigated fluorophores for *C. auris* under different growth conditions at different times. The proportions of fluorophores to dry mass were also calculated. Three or four measuring points are presented for each selected medium, whereby the concentrations determined are included in the curves in Figure 6, and the proportions of dry mass were also calculated.

YEPG medium					
Time [h]	OD600nm	Dry mass [mg/mL]	Determined concentration Fluoroph. [µg/mL]		Proportion to dry mass
20	0.93	22.0 ± 0.4	Rbf-eq.	$(316 \pm 1) \times 10^{-3}$	$(142 \pm 4) \times 10^{-7}$
			Lmc	$(146 \pm 7) \times 10^{-2}$	$(66 \pm 5) \times 10^{-6}$
			NADH	$(109 \pm 3) \times 10^{-0}$	$(50 \pm 15) \times 10^{-4}$
			PPIX	$(46 \pm 15) \times 10^{-1}$	$(21 \pm 8) \times 10^{-5}$
			ZnPP	$(222 \pm 14) \times 10^{-2}$	$(101 \pm 8) \times 10^{-6}$
			Copro III	$(67 \pm 14) \times 10^{-3}$	$(34 \pm 7) \times 10^{-7}$
			Thm	$(438 \pm 12) \times 10^{-1}$	$(20 \pm 1) \times 10^{-4}$
48	6.20	100 ± 4	Rbf-eq.	$(1061 \pm 5) \times 10^{-3}$	$(113 \pm 5) \times 10^{-7}$
			Lmc	$(542 \pm 18) \times 10^{-2}$	$(54 \pm 5) \times 10^{-6}$
			NADH	$(381 \pm 4) \times 10^{-0}$	$(383 \pm 19) \times 10^{-5}$
			PPIX	$(12 \pm 4) \times 10^{-0}$	$(13 \pm 5) \times 10^{-5}$
			ZnPP	$(70 \pm 6) \times 10^{-1}$	$(71 \pm 8) \times 10^{-6}$
			Copro III	$(14 \pm 4) \times 10^{-2}$	$(17 \pm 4) \times 10^{-7}$
			Thm	$(260 \pm 6) \times 10^{-0}$	$(261 \pm 16) \times 10^{-5}$
72	6.40	117 ± 4	Rbf-eq.	$(920 \pm 4) \times 10^{-3}$	$(84 \pm 3) \times 10^{-7}$
			Lmc	$(636 \pm 21) \times 10^{-2}$	$(54 \pm 4) \times 10^{-6}$
			NADH	$(325 \pm 20) \times 10^{-0}$	$(278 \pm 26) \times 10^{-5}$
			PPIX	$(100 \pm 50) \times 10^{-1}$	$(9 \pm 5) \times 10^{-5}$
			ZnPP	$(66 \pm 5) \times 10^{-1}$	$(56 \pm 6) \times 10^{-6}$
			Copro III	$(16 \pm 4) \times 10^{-2}$	$(13 \pm 3) \times 10^{-7}$
			Thm	$(162 \pm 12) \times 10^{-0}$	$(138 \pm 15) \times 10^{-5}$
Minimal medium + 10% NaCl					
Time [h]	OD600nm	Dry mass [mg/mL]	Determined concentration Fluoroph. [µg/mL]		Proportion to dry mass
22	0.023	0.43 ± 0.09	Rbf-eq.	$(113 \pm 4) \times 10^{-4}$	$(26 \pm 6) \times 10^{-6}$
			Lmc	$(50 \pm 6) \times 10^{-1}$	$(12 \pm 4) \times 10^{-3}$
			NADH	$(55 \pm 4) \times 10^{-0}$	$(13 \pm 4) \times 10^{-2}$
			PPIX	Not measurable	-
			ZnPP	$(54 \pm 18) \times 10^{-3}$	$(13 \pm 7) \times 10^{-5}$
			Copro III	Not measurable	-
			Thm	$(20 \pm 3) \times 10^{-0}$	$(47 \pm 16) \times 10^{-3}$

Continued on next page

Minimal medium + 10% NaCl					
Time [h]	OD600nm	Dry mass [mg/mL]	Determined concentration Fluoroph. [µg/mL]		Proportion to dry mass
44	0.17	10.63 ± 0.05	Rbf-eq.	$(1585 \pm 6) \times 10^{-4}$	$(154 \pm 2) \times 10^{-7}$
			Lmc	$(161 \pm 12) \times 10^{-1}$	$(151 \pm 12) \times 10^{-5}$
			NADH	$(131 \pm 13) \times 10^{-0}$	$(123 \pm 13) \times 10^{-4}$
			PPIX	$(413 \pm 16) \times 10^{-3}$	$(39 \pm 2) \times 10^{-6}$
			ZnPP	$(95 \pm 5) \times 10^{-2}$	$(89 \pm 5) \times 10^{-6}$
			Copro III	$(36 \pm 22) \times 10^{-3}$	$(3 \pm 2) \times 10^{-6}$
			Thm	$(76 \pm 7) \times 10^{-0}$	$(72 \pm 7) \times 10^{-4}$
72	0.28	29 ± 5	Rbf-eq.	$(1768 \pm 8) \times 10^{-4}$	$(6 \pm 1) \times 10^{-6}$
			Lmc	$(172 \pm 9) \times 10^{-2}$	$(59 \pm 13) \times 10^{-6}$
			NADH	$(100 \pm 40) \times 10^{-0}$	$(31 \pm 17) \times 10^{-4}$
			PPIX	$(354 \pm 18) \times 10^{-3}$	$(12 \pm 3) \times 10^{-6}$
			ZnPP	$(116 \pm 6) \times 10^{-2}$	$(39 \pm 8) \times 10^{-6}$
			Copro III	$(6 \pm 5) \times 10^{-2}$	$(2 \pm 1) \times 10^{-6}$
			Thm	$(752 \pm 12) \times 10^{-1}$	$(26 \pm 5) \times 10^{-4}$
160.5	0.20	11.53 ± 0.19	Rbf-eq.	$(1096 \pm 6) \times 10^{-4}$	$(110 \pm 2) \times 10^{-7}$
			Lmc	$(289 \pm 22) \times 10^{-1}$	$(251 \pm 23) \times 10^{-5}$
			NADH	$(139 \pm 15) \times 10^{-0}$	$(121 \pm 15) \times 10^{-4}$
			PPIX	$(95 \pm 13) \times 10^{-3}$	$(8 \pm 1) \times 10^{-6}$
			ZnPP	$(81 \pm 5) \times 10^{-2}$	$(70 \pm 5) \times 10^{-6}$
			Copro III	$(4 \pm 8) \times 10^{-2}$	$(3 \pm 7) \times 10^{-6}$
			Thm	$(114 \pm 12) \times 10^{-0}$	$(98 \pm 12) \times 10^{-4}$

4. Discussion

This study evaluates *C. auris* and the production of possible fluorophores under different growth conditions. In addition, the concentrations of the fluorophores examined in the aerobic experiments were determined in relation to dry mass over time. **Figure 2** presents the results of fluorescence spectroscopy of investigated fluorophores for various excitation wavelengths. The respective curve regression of the fluorophores agrees with the investigations of Koenig and Schneckenburger [33]. Additional information on the fluorescence properties of riboflavin equivalents and thiamine can be found in Yang et al. [34]. In the study of Kowalska and Kozik, the pathway of biosynthesis of thiamine is presented for yeast cells [35]. As was described in subsequent studies using porphyrins, it is important not to change the pH value or solutions for the entire measurements of fluorophores and yeast samples, as this has an influence on the fluorescence curves [18,36]. Since Laemmli buffer was used for *C. auris* samples in this study, but fluorophores had to be dissolved in other solvents beforehand, the proportions of DMSO and H_2O were kept as low as possible (**Table 1**) and later eliminated.

As described by Fyrestam et al., there are various factors that influence the production of different porphyrins [37]. In particular, the influence of growth conditions and time are described for bacteria. To investigate this for *C. auris*, two samples were cultivated aerobically with two different media (YEPG medium and minimal medium + 10 % NaCl). The results of the fluorescence spectroscopy are presented in **Figure 4**. Similar peaks were observed during growth with both media under aerobic conditions, whereby two additional peaks were detected by cultivating with minimal medium + 10 %

NaCl (575–585 nm and 630–640 nm). These peaks are due to an increased proportion of porphyrins (**Table 2**). For PPIX, more than twice the proportion to dry mass was determined for growth after 44 h with minimal medium + 10% NaCl than for growth in YEPG medium; for ZnPP, this was 1.3 times higher. The influence of the concentrations of endogenous porphyrins and zinc protoporphyrin under different growth conditions and strains of *Saccharomyces cerevisiae* was also investigated by Pretlow and Sherman [38]. They were able to detect different porphyrins in the yeast and described the concentrations of these substances under anaerobic growth conditions. The porphyrins investigated are formed via heme synthesis [39]. For this purpose, δ-aminolevulinic acid is first formed from glycine and succinyl-CoA. Both media contained peptone from casein as a source of amino acids. In the medium with an increased amount of nutrients, more substances such as thiamine and flavins formed. In the minimal medium, on the other hand, these substances can be less formed due to the low amount of nutrients, and more porphyrins are formed by the additional administration of peptone [40,41].

In order to investigate changes in the production of fluorophores over time, growth experiments were initially carried out under aerobic growth conditions with both media (**Figure 5**). The stationary phase was observed for the optimum medium after 50 h of cultivation, whereas this phase was reached after approximately 70 h for cultivation with the minimum medium + 10% NaCl.

All fluorophores analyzed were detected via simultaneous fluorescence spectroscopy. In the pathogenic relative *Candida albicans*, coproporphyrin, uroporphyrin, and flavins were detected using fluorescence spectroscopy [18,42]. When cultivated with YEPG medium, the concentration of PPIX did not decrease further after 50 h, and the concentration of Copro III increased (**Figure 6**). According to **Table 2**, the highest concentration was 12 ± 4 μg/mL for PPIX after 48 h and (16 ± 4) × 10^{-2} μg/mL for Copro III after 72 h. When comparing the proportion to dry mass, however, the highest proportions were observed after 20 h with (21 ± 8) × 10^{-5} for PPIX and (34 ± 7) × 10^{-7} for Copro III. In a study by Fyrestam et al., *Saccharomyces cerevisiae* was analyzed using high-performance liquid chromatography (HPLC), and a concentration of 2 ng/g was described for PPIX and 79 ng/g for Copro III [42]. Another study investigated the development of Copro III and PPIX over time using *Aggregatibacter actinomycetemcomitans* [37]. The results of the HPLC measurements described that, in contrast to the results for *C. auris*, the concentration of Copro III decreased and the concentration of PPIX increased.

When calculating the concentrations of different fluorophores in the yeast samples, the constant at the wavelength with the highest yield of fluorescence for each fluorophore (determined by the fit curve) was selected for further calculation across all excitation wavelengths. These constants A_n could then be multiplied by the concentrations of the pure chemical fluorophores. Due to the chosen superposition in **Formula 1**, the constants inherit the fluorescence yield of each fluorophore and describe the proportion they contribute to the whole spectrum. The approach of determining concentrations via fluorescence and measuring the pure chemicals beforehand was also described in the studies by Bohm et al. and Melø and Johnsson [43,44]. It is assumed that the yields of fluorescence of the previously measured fluorophores are equal to those in the sample to be compared if the analyzed fluorophores are present in the sample of the microorganism.

Clinical applications with endogenous PSs are described in different studies. Besides the irradiation of limb arthroplasty [45] or of biofilms on denture base resin [46,47] and in compact bone tissues [46], some diseases like candidal vaginitis are being investigated to be treated directly by irradiation [48].

A few studies have determined the combination of antifungal drugs and photoinactivation. It has been proven that a combinational treatment is better than a single method [49]. In particular, a reduced number of treatments with lower doses was described [50]. Additionally, a few works have shown that resistant microorganisms can re-gain their sensitivity against the applied drug [51,52].

5. Conclusions

In this study, 2D fluorescence spectroscopy was applied to investigate different aspects of *C. auris* growth. Various fluorophores and possible photosensitizers were detected. Different growth conditions could influence both the morphology and formation of fluorophores/possible PSs of *C. auris*. This could also be observed by changes in concentration over time. Since the formation of photosensitizers can be important for various therapeutic options like photodynamic therapy or phototherapy, this should be investigated further. In addition to other possible PSs, further growth conditions should also be examined for *C. aur*is and other pathogens.

Use of generative-AI tools declaration

The authors declare they have not used Artificial Intelligence (AI) tools in the creation of this article.

Conflict of interest

The authors declare no conflict of interest.

Author contributions

Conceptualization: A.-M.G. and M.H.; methodology, A.-M.G.; software, A.-M.G.; validation, A.-M.G., R.H. and M.H.; formal analysis, A.-M.G.; investigation, A.-M.G. and R.H.; resources, M.H.; data curation, A.-M.G.; writing—original draft preparation, A.-M.G.; writing—review and editing, A.-M.G., R.H., M.H.; visualization, A.-M.G.; supervision, M.H.; project administration, A.-M.G. and M.H.; funding acquisition, M.H. All authors have read and agreed to the published version of the manuscript.

References

1. Center for Disease Control and Prevention, Clinical alert to US healthcare facilities: global emergence of invasive infections caused by the multidrug-resistant yeast Candida auris, 2016. Available from: https://archive.cdc.gov/www_cdc_gov/fungal/candida-auris/candida-auris-alert.html.
2. Parums DV (2022) Editorial: The World Health Organization (WHO) fungal priority pathogens list in response to emerging fungal pathogens during the COVID-19 pandemic. *Med Sci Monit* 28: e939088. https://doi.org/10.12659/MSM.939088
3. Lockhart SR (2019) *Candida auris* and multidrug resistance: defining the new normal. *Fungal Genet Biol* 131: 103243. https://doi.org/10.1016/j.fgb.2019.103243

4. Ademe M, Girma F (2020) *Candida auris*: from multidrug resistance to pan-resistant strains. *Infect Drug Resist* 13: 1287–1294. https://doi.org/10.2147/IDR.S249864
5. Larkin E, Hager C, Chandra J, et al. (2017) The emerging pathogen *Candida auris*: growth phenotype, virulence factors, activity of antifungals, and effect of SCY-078, a novel glucan synthesis inhibitor, on growth morphology and biofilm formation. *Antimicrob Agents Ch* 61: 13. https://doi.org/10.1128/aac.02396-16
6. Wang X, Bing J, Zheng Q, et al. (2018) The first isolate of *Candida auris* in China: clinical and biological aspects. *Emerg Microbes Infec* 7: 93. https://doi.org/10.1038/s41426-018-0095-0
7. Fan S, Yue H, Zheng Q, et al. (2021) Filamentous growth is a general feature of *Candida auris* clinical isolates. *Med Mycol* 59: 734–740. https://doi.org/10.1093/mmy/myaa116
8. Tharp B, Zheng R, Bryak G, et al. (2023) Role of microbiota in the skin colonization of *Candida auris*. *mSphere* 8: e0062322. https://doi.org/10.1128/msphere.00623-22
9. Grice EA, Segre JA (2011) The skin microbiome. *Nat Rev Microbiol* 9: 244–253. https://doi.org/10.1038/nrmicro2537
10. Robinson S, Robinson AH (1954) Chemical composition of sweat. *Physiol Rev* 34: 202–220. https://doi.org/10.1152/physrev.1954.34.2.202
11. Baker LB (2019) Physiology of sweat gland function: the roles of sweating and sweat composition in human health. *Temperature (Austin)* 6: 211–259. https://doi.org/10.1080/23328940.2019.1632145
12. Eix EF, Nett JE (2022) Modeling *Candida auris* skin colonization: mice, swine, and humans. *Plos Pathog* 18: e1010730. https://doi.org/10.1371/journal.ppat.1010730
13. Satoh K, Makimura K, Hasumi Y, et al. (2009) *Candida auris* sp. nov., a novel ascomycetous yeast isolated from the external ear canal of an inpatient in a Japanese hospital. *Microbiol Immunol* 53: 41–44. https://doi.org/10.1111/j.1348-0421.2008.00083.x
14. Sakamoto FH, Lopes JD, Anderson RR (2010) Photodynamic therapy for acne vulgaris: a critical review from basics to clinical practice: part I. Acne vulgaris: when and why consider photodynamic therapy? *J Am Acad Dermatol* 63: 183–193. https://doi.org/10.1016/j.jaad.2009.09.056
15. Yang F, Xu M, Chen X, et al. (2023) Spotlight on porphyrins: classifications, mechanisms and medical applications. *Biomed Pharmacother* 164: 114933. https://doi.org/10.1016/j.biopha.2023.114933
16. Barron GA, Moseley H, Woods JA (2013) Differential sensitivity in cell lines to photodynamic therapy in combination with ABCG2 inhibition. *J Photochem Photobiol B* 126: 87–96. https://doi.org/10.1016/j.jphotobiol.2013.07.003
17. Harris DM, Werkhaven J (1987) Endogenous porphyrin fluorescence in tumors. *Lasers Surg Med* 7: 467–472. https://doi.org/10.1002/lsm.1900070605
18. Plavskii VY, Mikulich AV, Tretyakova AI, et al. (2018) Porphyrins and flavins as endogenous acceptors of optical radiation of blue spectral region determining photoinactivation of microbial cells. *J Photochem Photobiol B* 183: 172–183. https://doi.org/10.1016/j.jphotobiol.2018.04.021
19. Hessling M, Wenzel U, Meurle T, et al. (2020) Photoinactivation results of *Enterococcus moraviensis* with blue and violet light suggest the involvement of an unconsidered photosensitizer. *Biochem Biophy Rese Co* 533: 813–817. https://doi.org/10.1016/j.bbrc.2020.09.091

20. Gierke AM, Hessling M (2024) Photoinactivation by UVA radiation and visible light of *Candida auris* compared to other fungi. *Photochem Photobiol Sci* 23: 681–692. https://doi.org/10.1007/s43630-024-00543-4
21. Pallotta ML (2011) Evidence for the presence of a FAD pyrophosphatase and a FMN phosphohydrolase in yeast mitochondria: a possible role in flavin homeostasis. *Yeast* 28: 693–705. https://doi.org/10.1002/yea.1897
22. Viñas P, Balsalobre N, López-Erroz C, et al. (2004) Liquid chromatographic analysis of riboflavin vitamers in foods using fluorescence detection. *J Agric Food Chem* 52: 1789–1794. https://doi.org/10.1021/jf030756s
23. Zhao C, Liu L, Ge J, et al. (2017) Ultrasensitive determination for flavin coenzyme by using a ZnO nanorod photoelectrode in a four-electrode system. *Microchim Acta* 184: 2333–2339. https://doi.org/10.1007/s00604-017-2230-3
24. Hu X, Huang YY, Wang Y, et al. (2018) Antimicrobial photodynamic therapy to control clinically relevant biofilm infections. *Front Microbiol* 9: 1299. https://doi.org/10.3389/fmicb.2018.01299
25. Plaetzer K, Krammer B, Berlanda J, et al. (2009) Photophysics and photochemistry of photodynamic therapy: fundamental aspects. *Lasers Med Sci* 24: 259–268 https://doi.org/10.1007/s10103-008-0539-1
26. Di Meo S, Reed TT, Venditti P, et al. (2016) R Role of ROS and RNS sources in physiological and pathological conditions *Oxid Med Cell Longev* 2016: 1245049. https://doi.org/10.1155/2016/1245049
27. Mallidi S, Anbil S, Lee S, et al. (2014) Photosensitizer fluorescence and singlet oxygen luminescence as dosimetric predictors of topical 5-aminolevulinic acid photodynamic therapy induced clinical erythema. *J Biomed Opt* 19: 028001. https://doi.org/10.1117/1.JBO.19.2.028001
28. Brasch J, Kay C (2006) Effects of repeated low-dose UVB irradiation on the hyphal growth of *Candida albicans*. *Mycoses* 49: 1–5. https://doi.org/10.1111/j.1439-0507.2005.01169.x
29. Cieplik F, Späth A, Leibl C, et al. (2014) Blue light kills *Aggregatibacter actinomycetemcomitans* due to its endogenous photosensitizers. *Clin Oral Investi* 18: 1763–1769. https://doi.org/10.1007/s00784-013-1151-8
30. Lei J, Huang J, Xin C, et al. (2023) Riboflavin targets the cellular metabolic and ribosomal pathways of *Candida albicans in vitro* and exhibits efficacy against oropharyngeal candidiasis. *Microbiol Spectr* 11: e0380122. https://doi.org/10.1128/spectrum.03801-22
31. Oriel S, Nitzan Y (2010) Photoinactivation of *Candida albicans* by its own endogenous porphyrins. *Curr Microbiol* 60: 117–123. https://doi.org/10.1007/s00284-009-9514-8
32. Meir Z, Osherov N (2018) Vitamin biosynthesis as an antifungal target. *J Fungi (Basel)* 4: 72. https://doi.org/10.3390/jof4020072
33. Koenig K, Schneckenburger H (1994) Laser-induced autofluorescence for medical diagnosis. *J Fluoresc* 4: 17–40. https://doi.org/10.1007/BF01876650
34. Yang H, Xiao X, Zhao X S, et al. (2016) Study on fluorescence spectra of thiamine and riboflavin. *MATEC Web Conf* 63: 03013. https://doi.org/10.1051/matecconf/20166303013
35. Kowalska E, Kozik A (2008) The genes and enzymes involved in the biosynthesis of thiamin and thiamin diphosphate in yeasts. *Cell Mol Biol Lett* 13: 271–282. https://doi.org/10.2478/s11658-007-0055-5

36. Maitra D, Pinsky BM, Soherawardy A, et al. (2021) Protein-aggregating ability of different protoporphyrin-IX nanostructures is dependent on their oxidation and protein-binding capacity. *J Biol Chem* 297: 100778. https://doi.org/10.1016/j.jbc.2021.100778
37. Fyrestam J, Bjurshammar N, Paulsson E, et al. (2017) Influence of culture conditions on porphyrin production in *Aggregatibacter actinomycetemcomitans* and *Porphyromonas gingivalis*. *Photodiagn Photodyn* 17: 115–123. https://doi.org/10.1016/j.pdpdt.2016.11.001
38. Pretlow TP, Sherman F (1967) Porphyrins and zinc porphyrins in normal and mutant strains of yeast. *BBA–Gen Subjects* 148: 629–644. https://doi.org/10.1016/0304-4165(67)90036-0
39. Phillips JD (2019) Heme biosynthesis and the porphyrias. *Mol Genet Metab* 128: 164–177. https://doi.org/10.1016/j.ymgme.2019.04.008
40. Andrawes N, Weissman Z, Pinsky M, et al. (2022) Regulation of heme utilization and homeostasis in *Candida albicans*. *Plos Genet* 18: e1010390. https://doi.org/10.1371/journal.pgen.1010390
41. Kornitzer, D.; Roy, U. (2020) Pathways of heme utilization in fungi. *Biochim Biophys Acta Mol Cell Res* 1867: 118817. https://doi.org/10.1371/journal.pgen.1010390
42. Harris DM (2023) Spectra of pathogens predict lethality of blue light photo-inactivation. *Laser Ther J* 30: 314. http://dx.doi.org/10.4081/ltj.2023.314
43. Bohm GC, Gandara L, Di Venosa G, et al. (2020) Photodynamic inactivation mediated by 5-aminolevulinic acid of bacteria in planktonic and biofilm forms. *Biochem Pharmacol* 177: 114016. https://doi.org/10.1016/j.bcp.2020.114016
44. Melø TB, Johnsson M (1982) In vivo porphyrin fluorescence for *Propionibacterium acnes*. A characterization of the fluorescing pigments. *Dermatologica* 164: 167–174. https://doi.org/10.1159/000250086
45. Gupta S, MacLean M, Anderson JG, et al. (2015) Inactivation of micro-organisms isolated from infected lower limb arthroplasties using high-intensity narrow-spectrum (HINS) light. *Bone Joint J* 97: 283–288. https://doi.org/10.1302/0301-620X.97B2.35154
46. Rosa LP, Da Silva FC, Viana MS, et al. (2016) In vitro effectiveness of 455-nm blue LED to reduce the load of *Staphylococcus aureus* and *Candida albicans* biofilms in compact bone tissue. *Lasers Med Sci* 31: 27–32. https://doi.org/10.1007/s10103-015-1826-2
47. Tsutsumi-Arai C, Arai Y, Terada-Ito C, et al. (2022) Microbicidal effect of 405-nm blue LED light on *Candida albicans* and *Streptococcus mutans* dual-species biofilms on denture base resin. *Lasers Med Sci* 37: 857–866. https://doi.org/10.1007/s10103-021-03323-z
48. Wang T, Dong J, Yin H, et al. (2020) Blue light therapy to treat candida vaginitis with comparisons of three wavelengths: an in vitro study. *Lasers Med Sci* 35: 1329–1339. https://doi.org/10.1007/s10103-019-02928-9
49. Pérez-Laguna V, García-Luque I, Ballesta S, et al. (2021) Photodynamic therapy combined with antibiotics or antifungals against microorganisms that cause skin and soft tissue infections: A planktonic and biofilm approach to overcome resistances. *Pharmaceuticals* 14: 603. https://doi.org/10.3390/ph14070603
50. Pérez-Laguna V, Gilaberte Y, Millán-Lou MI, et al. (2019) A combination of photodynamic therapy and antimicrobial compounds to treat skin and mucosal infections: a systematic review. *Photochem Photobiol Sci* 18: 1020–1029. https://doi.org/10.1039/c8pp00534f
51. Wozniak A, Rapacka-Zdonczyk A, Mutters NT, et al. (2019) Antimicrobials are a photodynamic iinactivation adjuvant for the eradication of extensively drug-resistant *Acinetobacter baumannii*. *Front Microbiol* 10: 229. https://doi.org/10.3389/fmicb.2019.00229

52. Ilizirov Y, Formanovsky A, Mikhura I, et al. (2018) Effect of photodynamic antibacterial chemotherapy combined with antibiotics on gram-positive and gram-negative bacteria. *Molecules* 23: 3152. https://doi.org/10.3390/molecules23123152

AIMS Press